Rotational analysis of the $\tilde{B}\,^2\Sigma^+$–$\tilde{X}\,^2\Sigma^+$ transition of BaOH and BaOD

S. Kinsey-Nielsen, C. R. Brazier, and P. F. Bernath
Department of Chemistry, University of Arizona, Tucson, Arizona 85721

(Received 2 August 1985; accepted 11 October 1985)

The $\tilde{B}\,^2\Sigma^+$–$\tilde{X}\,^2\Sigma^+$ transitions of BaOH and BaOD were studied by the technique of dye laser spectroscopy. The 000–000 and 001–000 bands of BaOH and 000–000 band of BaOD were rotationally analyzed. The $\tilde{B}\,^2\Sigma^+$ state is perturbed by the $\tilde{A}\,^2\Pi$ state and each parity (e/f) component of the B state was fit separately. BaOH is a linear molecule with r_0(Ba–O) = 2.201 Å and r_0(O–H) = 0.923 Å. The $\tilde{X}\,^2\Sigma^+$ vibrational frequencies for BaOH (BaOD) are 492.4 (482.4) cm^{-1} for Ba–O stretch and 341.6 (257.6) cm^{-1} for the bend.

I. INTRODUCTION

Alkaline earth monohydroxides are found in a variety of energetic environments including flames[1] and stellar atmospheres.[2,3] It is speculated that alkaline earth monohydroxides are formed in the upper atmosphere[4] from metals and ions released either by man[5] or by ablation from meteors.[6,7] These radicals might potentially be found in the interstellar medium where they may be produced by ion–electron recombination[8] or metal ion reactions on surfaces.[9]

When an alkaline earth salt is added to a flame, a characteristic visible emission spectrum appears. The dominant molecular contribution is due to the metal monohydroxide. Alkaline earth flame spectra date back to observations by Herschel[10] in 1823. In 1955 James and Sugden[11] correctly assigned the carrier of the flame bands to the alkaline earth monohydroxides by noting the close similarity to alkaline earth monohalides (OH^- behaves like a pseudohalide). The observation of a deuterium isotope effect by Charton and Gaydon[12,13] helped to confirm this assignment. Since then numerous additional flame investigations[14–18] have been undertaken because of the importance of flame emission and absorption in analytical chemistry. The addition of small amounts of alkaline earth salts has a dramatic effect on flame chemistry[19] by catalyzing radical–radical recombination[20] and (for Ba) suppressing soot production in fuel rich flames.[21] In an environment rich in hydrogen and oxygen, the alkaline earth monohydroxides are the dominant metal containing species because of their large dissociation energies.

The dissociation energies[1,22,23] and ionization potentials[24,25] of the alkaline earth monohydroxides can be derived from flame equilibrium studies. More recently Murad[26] has directly determined these quantities by high temperature mass spectroscopy. The dissociation energy was established by the mass spectrometric determination of the equilibrium composition of the H_2 + MO system while the appearance potentials provided estimates of the ionization energies. Flame,[27] ion beam,[28] and flowing afterglow[29] studies of the chemistry of some of the alkaline earth monohydroxide ions have also been published.

The electron spin resonance (ESR) spectra of BeOH and MgOH were analyzed by Brom and Weltner.[30] Even for BeOH, the spectra could be interpreted as arising from linear, ionically bonded species (M^+–OH^-) with the unpaired spin density residing on the metal. The theoretical work of Hinchliffe[31] supports these observations for BeOH and MgOH. Additional *ab initio* calculations for BeOH and MgOH were made by Abashkin and Dement'ev,[32] Palke and Kirtman,[33] while Bauschlicher and Partridge[34] have computed the dissociation energy of CaOH. Additional theoretical calculations (especially for excited electronic states) would certainly be helpful in more thoroughly characterizing the electronic structure of the alkaline earth monohydroxides.

Infrared spectra of some matrix-isolated alkaline earth monohydroxides were observed by Kauffman, Hauge, and Margrave.[35] They discovered that codeposition of metal and water in an argon matrix at 15 K produced $M \cdot OH_2$ complexes. Upon photolysis M inserted in an OH bond to produce H–M–OH and under prolonged UV photolysis MOH was formed for Sr and Ba.

In addition to flame sources, the MgOH molecule was made in an electric arc through water with magnesium electrodes[36] or in a King furnace.[37] However, the most important advance was the discovery that alkaline earth monohydroxides[38,39] could be made in a Broida-type oven.[40] The combination of a cool ($\simeq$500 K) molecular source and the technique of laser excitation spectroscopy with narrow band fluorescence detection allowed Harris and co-workers to undertake the first high resolution studies.[41,42]

Hilborn, Zhu, and Harris[41] analyzed the $\tilde{A}\,^2\Pi$–$\tilde{X}\,^2\Sigma^+$ transition of CaOH while Nakagawa, Wormsbecher, and Harris[42] tackled the $\tilde{B}\,^2\Sigma^+$–$\tilde{X}\,^2\Sigma^+$ system of SrOH. The $\tilde{B}\,^2\Sigma$–$\tilde{X}\,^2\Sigma^+$ studies[43] and additional work on the $\tilde{A}\,^2\Pi$–$\tilde{X}\,^2\Sigma^+$ system[44] of CaOH were completed in our laboratory. In addition to laser excitation spectroscopy, we detected laser induced fluorescence from the $\tilde{A}\,^2\Pi$–$\tilde{X}\,^2\Sigma^+$ transition of SrOH by Fourier transform spectroscopy.[45] We now report on the $\tilde{B}\,^2\Sigma^+$–$\tilde{X}\,^2\Sigma^+$ transition of BaOH and BaOD, observed for the first time at high resolution.

The isoelectronic BaF[46,47] molecule served as a useful guide to the BaOH spectrum. As for the (CaOH, CaF) and (SrOH, SrF) pairs the electronic, vibrational, rotational, and fine structure (spin-rotation, Λ-doubling) molecular parameters transfer systematically from the diatomic to the triatomic. The $\tilde{B}\,^2\Sigma^+$–$\tilde{X}\,^2\Sigma^+$ transition[46] of BaF is relatively simple and well characterized but the corresponding BaOH transition provided unanticipated complications because of

 0021-9606/86/020698-11$02.10

extensive sequence structure and severe perturbations present in the $\tilde{B}\,^2\Sigma^+$ state.

II. METHOD

The BaOH and (BaOD) molecules were made in a Broida-type oven.[40] Briefly, Ba metal was vaporized from a resistively heated alumina crucible, entrained in an Ar carrier flow, and allowed to react with a few millitorr of H_2O (D_2O) vapor. The amount of molecule produced was enhanced by decreasing the pumping speed until the total pressure in the oven was approximately 9 Torr.

The 9 W, 5145 Å output of a Coherent Innova 20 argon-ion laser was used to pump a Coherent 699-29 computer-controlled ring dye laser operated near 7580 Å with pyridine 2 dye. Laser-induced fluorescence was observed when the resulting 100–200 mW laser beam was focused into the BaOH (BaOD) flame. BaOD data collection was complicated by working at the red edge of both the dye gain curve and the dye laser's wavemeter.

Initially, the dye laser was used broadband (1 cm^{-1} bandwidth) to make vibrational assignments. The laser was scanned while the total fluorescence and filtered fluorescence were recorded on a two-pen chart recorder. The latter was collected by focusing the fluorescence onto the slits of a 0.64 m monochromator (slits set to provide 1 Å resolution unless otherwise noted) and detecting with a cooled photomultiplier tube (RCA C31034) using photon counting electronics. The monochromator was set at 8250 Å ($\tilde{A}\,^2\Pi_{3/2}$–$\tilde{X}\,^2\Sigma^+$) to allow observation of the $\tilde{B}\,^2\Sigma^+$–$\tilde{X}\,^2\Sigma^+$ transition (collisions connect the $\tilde{A}$ and $\tilde{B}$ states). Detection of the $\tilde{B}\,^2\Sigma^+$–$\tilde{X}\,^2\Sigma^+$ by monitoring the $\tilde{A}\,^2\Pi_{3/2}$–$\tilde{X}\,^2\Sigma^+$ greatly reduced the scattered laser light. These laser excitation scans provided a clear pattern of R bandheads for the $\tilde{B}\,^2\Sigma^+$–$\tilde{X}\,^2\Sigma^+$ transition. Resolved fluorescence scans were also recorded by fixing the laser on a bandhead and scanning the monochromator.

Next, the dye laser was converted to single mode operation (1 MHz bandwidth) to observe rotational structure. The high-resolution total fluorescence and filtered fluorescence spectra were recorded on the computer as the laser was scanned. Rotational lines were recorded by setting the monochromator in the P or R branch and scanning the laser in the corresponding R or P branch. Although the total fluorescence channel usually provided resolved lines, the filtered fluorescence channel simplified the spectra and insured proper tracking of the rotational lines.[48,49] Rotational assignments were made by setting the monochromator (slits set for 0.2 Å resolution) on a specific P or R line, scanning the laser in the corresponding R or P branch, and detecting the single connecting R or P line. Combination differences of the connecting lines provided a definite rotational assignment.

Finally, vibrational frequencies were determined by setting the single frequency dye laser on a specific rotational line and dispersing the fluorescence with the monochromator. These resolved fluorescence scans provided ground state vibrational frequencies for the Ba–O stretch and the bend as well as some $\tilde{A}\,^2\Pi$–$\tilde{X}\,^2\Sigma^+$ lines produced by $\tilde{B}\,^2\Sigma^+$–$\tilde{A}\,^2\Pi$ cascade.

A thorium hollow cathode lamp was used in a laser optogalvanic experiment to provide absolute wavelength calibration.[50] The conditions used were similar to those of Sansonetti and Weber[51]: 15 mA discharge current; 15 mW laser power; 1110 Hz chopping frequency; 0.1 μF coupling capacitor; 5 kΩ ballast resistor; and no lens. A few strong lines were recorded at the beginning and end of each day to check the dye laser wavemeter calibration. The absolute accuracy of our line positions is approximately ± 0.003 cm^{-1}.

III. RESULTS AND ANALYSIS

A. Vibrational analysis

Figures 1 and 2 are laser excitation spectra of the $\tilde{B}\,^2\Sigma^+$–$\tilde{X}\,^2\Sigma^+$ transitions of BaOH and BaOD, respectively.

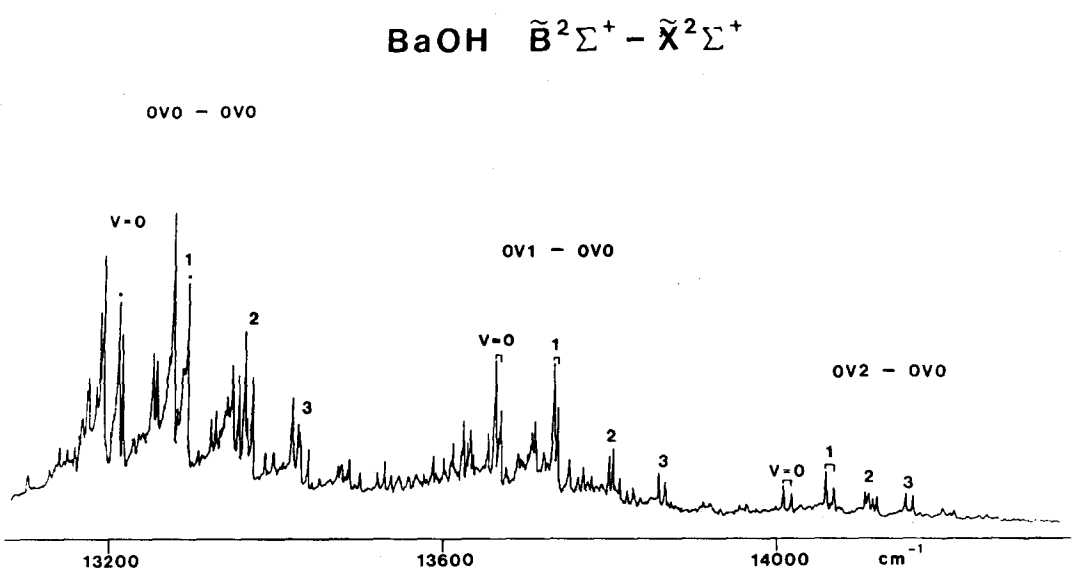

FIG. 1. BaOH laser excitation spectrum. The broadband dye laser was scanned with the monochromator at 8250 Å ($\tilde{A}\,^2\Pi$–$\tilde{X}\,^2\Sigma^+$ emission, see the text). The filtered fluorescence shows the prominent R bandheads (R_1 and R_2 for each band) and complicated vibrational structure.

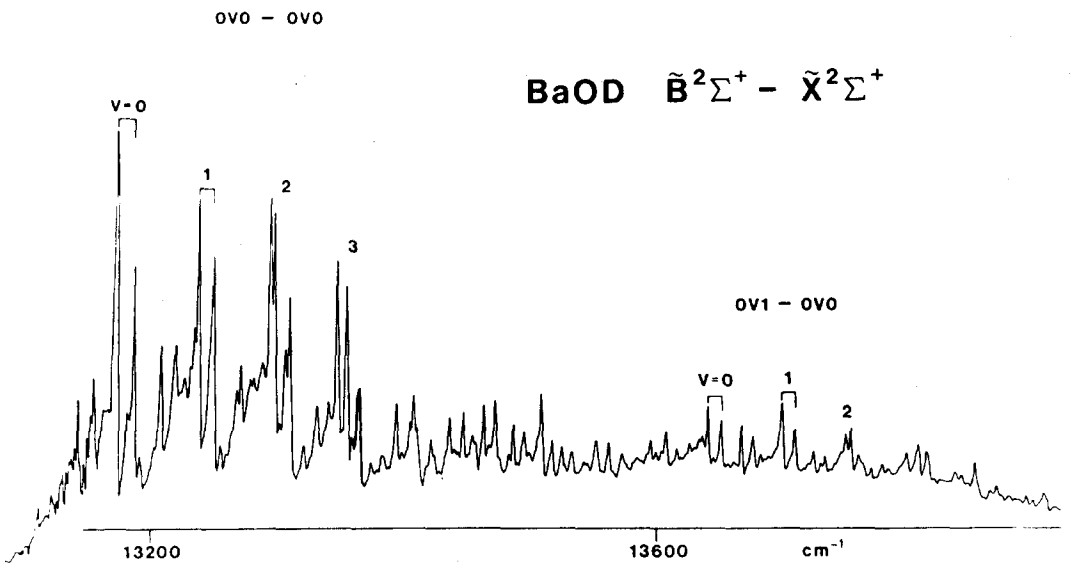

FIG. 2. BaOD laser excitation spectrum. The broadband dye laser was scanned, and the total fluorescence was detected.

Each scan shows a complicated pattern of doubled R branch bandheads with extensive sequence structure. An attempt was made to assign as many bands as possible to activity in the Ba–O stretch (ν_3) and Ba–O–H bend (ν_2). Note that this numbering of the vibrational modes differs from previous papers but is now consistent with the recommended notation.[52]

As for BaF, the bands are double headed because of the large spin-rotation constant in the $\tilde{B}\,^2\Sigma^+$ state. In general, the R_1 heads are to the red of the R_2 heads. For some bands, such as 000–000 and 010–010 of BaOH, the splitting is not resolved (Fig. 1). There are many extra features in the spectra, such as the sharp peak just to the blue of the R_1 and R_2 000–000 BaOH heads (Fig. 1). We believe these extra features are $\tilde{A}\,^2\Pi$–$\tilde{X}\,^2\Sigma^+$ bandheads appearing because of $\tilde{B}\,^2\Sigma^+$–$\tilde{A}\,^2\Pi$ perturbations. The combination of dense sequence structure, a doubly degenerate bend (producing vibrational angular momentum) and perturbations results in the formidable appearance of Figs. 1 and 2.

The vibrational pattern is a progression in the Ba–O stretch: $\Delta v_3 = 0$, $\Delta v_3 = 1$, $\Delta v_3 = 2$. Within each group of bands with the same Δv_3 there is sequence structure due to the bend (e.g., for the $\Delta v_3 = 1$ group: 001–000, 011–010, 021–020, etc. bands proceeding to the blue). In addition, each Δv_3 group has a weaker sequence structure due to ν_3 (e.g., for the $\Delta v_3 = 0$ group: 000–000, 001–001, 002–002...; 010–010, 011–011, 012–012, etc. bands proceeding to the red).

The results of our bandhead analysis are listed in Table I. Some of the bandheads were measured directly with the monochromator (± 1 Å accuracy). Most of the measurements involved interpolating the excitation scan (at best ± 2 Å accuracy). More accurate bandhead measurements (± 0.005 Å accuracy) were made for the three bands that were rotationally analyzed (see the next section). The bandhead–band origin spacings are large and somewhat erratic because of the effect of $\tilde{B}\,^2\Sigma^+ \sim \tilde{X}\,^2\Pi^+$ perturbations on the large spin-rotation parameter of the $\tilde{B}$ state.

After the rotational analyses were completed (see the next section), ground state vibrational frequencies were obtained for BaOH and BaOD by setting the single mode dye laser on individual rotational lines and recording the resolved fluorescence through the monochromator. Figure 3 shows a BaOH resolved fluorescence scan with the laser on

TABLE I. Bandheads for the $\tilde{B}\,^2\Sigma^+$–$\tilde{X}\,^2\Sigma^+$ transitions of BaOH and BaOD (in Å). Unless otherwise noted, numbers are reported with ± 2 Å accuracy.

	BaOH					BaOD	
	$v=0$	1	2	3	4	$v=0$	1
0v0–0v0 R_1	7567.876[a]	7521[b]	7480	7441	...	7586.961[a]	7552
R_2	7568.282[a]	7521[b]	7475	7436	7405	7579.466[a]	7546
0v1–0v1 R_1	7578	7531[b]	7489	7447			
R_2	7578	7531[b]	7484	7443			
0v1–0v0 R_1	7315.430[a]	7273	7240	7212[b]		7336	7306
R_2	7311.466[a]	7271	7237	7208[b]		7331	7300
0v2–0v0 R_1	7134[b]	7108[b]					
R_2	7130[b]	7104[b]					

[a] Measured to ± 0.005 Å accuracy.
[b] Measured to 1 Å accuracy.

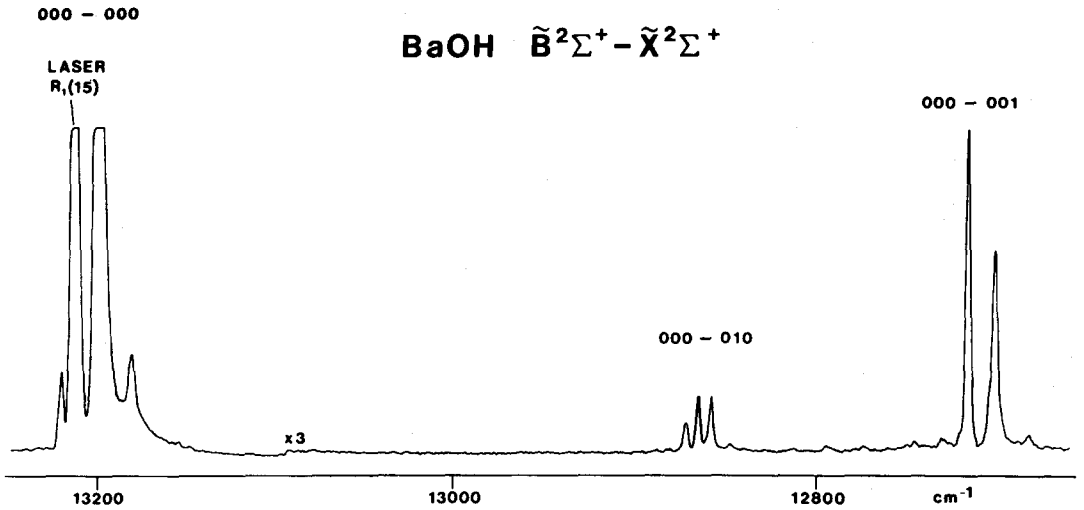

FIG. 3. BaOH resolved fluorescence spectrum. The monochromator was scanned with the single frequency dye laser on the $R_1(15)$ rotational line of the 000–000 band (13 205.177 cm^{-1}). The nominally forbidden 000–010 band arises from the perpendicular character present in the parallel $\tilde{B}$–$\tilde{X}$ transition.

the $R_1(15)$ line of the 000–000 band (13 205.777 cm^{-1}). In this spectrum the 000–010 and 000–001 band emission provide the Ba–O–H bend (341.6 cm^{-1}) and the Ba–O stretch (492.4 cm^{-1}) for the $\tilde{X}\,^2\Sigma^+$ state. Figure 4 shows the resolved fluorescence scan for BaOD where, in this case, the laser was resonant with the $R_2(6)$ line of the 000–000 band (13 177.318 cm^{-1}). The Ba–O–D bend (257.6 cm^{-1}) has a lower frequency than the Ba–O–H bend while the Ba–O stretch (482.4 cm^{-1}) is approximately the same for both molecules. Twice the Ba–O–D bend (501.0 cm^{-1}) was partially obscured by the stretch. In both molecules, transitions with $\Delta v_2 = 1$ were unambiguously identified because of the PQR structure that arises from a perpendicular transition. The BaOH excited state stretch, ν_3', was determined from the energy difference between the 000–000 and 001–000 band origins. All observed vibrational frequencies are listed in Table II.

B. Rotational analysis

Three bands were rotationally analyzed: the 000–000 and 001–000 bands of BaOH; and the 000–000 band of BaOD. Figure 5 shows an example of a typical high-resolution laser excitation spectrum. The BaOH 000–000 band R_1 branch lines were observed by scanning the single frequency dye laser with the monochromator in the P_1 branch (7584.3 Å). The filtered fluorescence shows individual rotational lines rather than overlapped lines.

The measured rotational lines for the three bands analyzed are listed in Tables III, IV, and V. A local perturbation was observed in the R_2 branch of the BaOD band at $N'' = 37$–42. Unfortunately, it was not possible to obtain corresponding high N P_2 (or more than a few P_1) lines because the dye laser was at the red limit of its operating range and performed very erratically.

A nonlinear least squares fit of the lines of Tables III–V

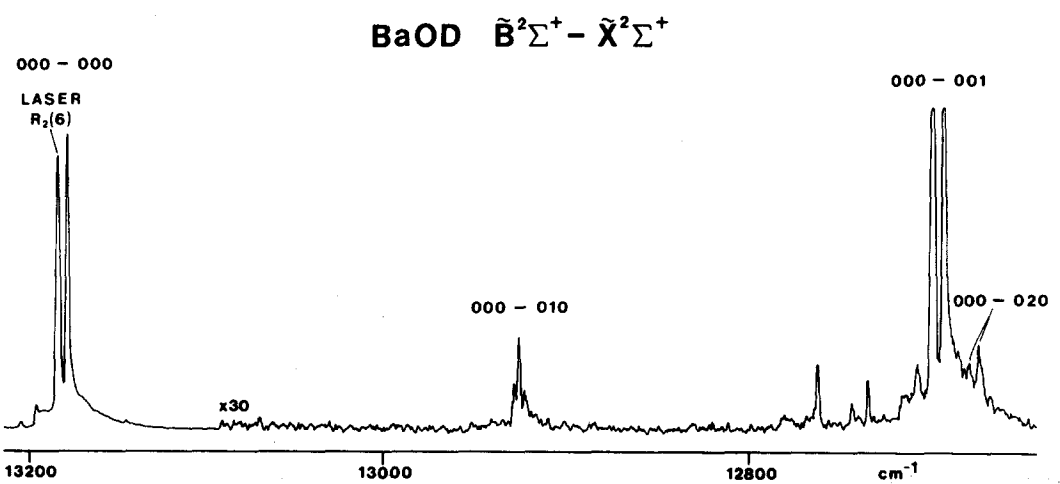

FIG. 4. BaOD resolved fluorescence spectrum. The monochromator was scanned with the single frequency dye laser on the $R_2(6)$ rotational line of the 000–000 band (13 177.318. cm^{-1}). Notice that the ground state bend (257.6 cm^{-1}) is considerably smaller than for BaOH while the Ba–O stretch (482.4 cm^{-1}) is approximately the same. Twice the bend (501.0 cm^{-1}) is partially obscured by the Ba–O stretch fundamental.

TABLE II. Vibrational frequencies for BaOH and BaOD (in cm^{-1}).

	$\tilde{X}\,^2\Sigma^+$	
	BaOH	BaOD
ν_2	341.6(6)[a]	257.6(4)
$2\nu_2$	661.1(6)	501.0(5)
$3\nu_2$		734.4(4)
ν_3	492.4(8)	482.4(2)
	$\tilde{B}\,^2\Sigma^+$	
ν_3	461.0(3)	

[a] Numbers in parentheses correspond to one standard deviation in the last digit.

was accomplished using the customary $^2\Sigma$ energy level expressions.[53] Unfortunately, it was found that the e and f levels[54] of the $\tilde{B}\,^2\Sigma^+$ state could not be fit together with a single spin-rotation parameter, γ. The $\tilde{X}\,^2\Sigma^+$ states for both BaOH and BaOD are well behaved with the expected $P_1 - R_1$ and $P_2 - R_2$ combination differences. The expressions for ground state combination differences are[53]:

$$\text{for } e \quad \Delta_2 F_1(N) = 4B_v(N + 1/2) + \gamma,$$

$$\text{for } f \quad \Delta_2 F_2(N) = 4B_v(N + 1/2) - \gamma.$$

By assuming γ'' to be positive, e and f levels can be distinguished. For the $\tilde{B}\,^2\Sigma^+$ states the e and f levels behave as if each were a different electronic state with different molecular constants. For BaOH all of the constants are reasonably similar except γ', while for BaOD even the B' values are different. It is possible that the e and f levels do, in fact, belong to different vibronic states, especially for the strongly perturbed BaOD molecule, but a careful search disclosed no other strong transitions nearby. A more likely explanation is that a strong parity dependent perturbation has affected the e levels in a different way than the f levels.

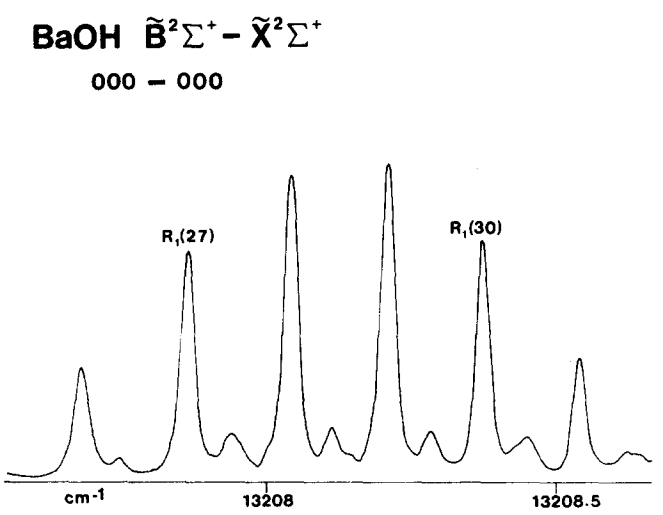

FIG. 5. High-resolution BaOH spectrum. This is a section of the laser excitation spectrum of the R_1 branch of the 000–000 band. The single frequency dye laser was scanned in the R_1 branch with the monochromator at 7584.3 Å (P_1 branch). The monochromator acts as a narrow bandpass filter to select lines of interest.

The observed BaOH transition wave numbers (Tables III and IV) were simultaneously fit with five effective states in the Hamiltonian: $\tilde{X}\,^2\Sigma^+$ 000; $\tilde{B}\,^2\Sigma^+$ 000e; $\tilde{B}\,^2\Sigma^+$ 000f; $\tilde{B}\,^2\Sigma^+$ 001e; and $\tilde{B}\,^2\Sigma^+$ 001f. The BaOD transitions (Table V) were fit with three states: $\tilde{X}\,^2\Sigma^+$ 000; $\tilde{B}\,^2\Sigma^+$ 000e; and $\tilde{B}\,^2\Sigma^+$ 000f. The molecular parameters from these fits are reported in Table VI for BaOH and Table VII for BaOD. Often for $^2\Sigma$–$^2\Sigma$ transitions γ'' and γ' are badly, but not completely, correlated. Because of the small number of P branch lines for BaOD, γ'' could not be determined and was fixed to 0.002 44 cm^{-1}. This estimated value was obtained by multiplying γ''(BaOH) = 0.002 70 cm^{-1} (Table VI) by the ratio of B'' (BaOD) to B'' (BaOH) (Tables VII and VI, respectively). The more extensive data for BaOH, including the presence of two vibrational bands in the fit, allowed γ'' to be determined.

The $\tilde{B}\,^2\Sigma^+$–$\tilde{X}\,^2\Sigma^+$ rotational analysis indicates that BaOH is a linear molecule like the other alkaline earth monohydroxides. The ground state rotational constants for BaOH and BaOD provide an r_0 structure. Using B''_{000} (BaOH) = 0.216 571 cm^{-1}, and B''_{000} (BaOD) = 0.195 743 cm^{-1}, the ground state r_0 values were calculated to be 2.201 Å for the Ba–O and 0.923 Å for the O–H (D) bond lengths.

C. $\tilde{A}\,^2\Pi$–$\tilde{X}\,^2\Sigma^+$ transition

When the single frequency dye laser was set on the $R_1(15)$ line of the BaOH $\tilde{B}\,^2\Sigma^+$–$\tilde{X}\,^2\Sigma^+$ 000–000 band (13 205.177 cm^{-1}) in order to determine the ground state vibrational frequencies, resonance fluorescence of the $\tilde{A}\,^2\Pi$–$\tilde{X}\,^2\Sigma^+$ transition was also observed. Figure 6 shows the observed $\tilde{A}$–$\tilde{X}$ emission spectrum, observed because of a resonant $\tilde{B}$–$\tilde{A}$–$\tilde{X}$ cascade. A number of unresolved but assignable rotational lines in the $\tilde{A}$–$\tilde{X}$ 000–000 band were seen for both the $^2\Pi_{3/2}$ and $^2\Pi_{1/2}$ spin components. The spin-orbit splitting parameter, A, was found to be 635 $\pm$ 1 cm^{-1} from these lines. The origins were estimated to be $T_0(^2\Pi_{3/2})$ = 12 207 $\pm$ 1 cm^{-1} and $T_0(^2\Pi_{1/2})$ = 11 572 $\pm$ 1 cm^{-1}. The strong fluorescence to the red of each set of $\tilde{A}$–$\tilde{X}$ 000–000 lines probably represents diagonal emission from higher vibrational levels of the $\tilde{A}\,^2\Pi$ state. Presumably, these levels are resonantly populated by collisions from the 000 level of $\tilde{B}\,^2\Sigma^+$.

IV. DISCUSSION

A. Chemistry

The production of $\tilde{X}\,^2\Sigma^+$ BaOH molecules via the direct reaction,

$$\text{Ba}(g) + H_2O \rightarrow \text{BaOH} + H,$$

is endothermic by approximately 12 kcal/mol. Therefore, it is unlikely that the majority of BaOH produced is a result of the direct reaction pathway.

We can imagine two possible mechanisms for BaOH production each involving the formation of a H–Ba–OH intermediate:

TABLE III. The measured lines of the BaOH 000–000 $\tilde{B}\,^2\Sigma^+$–$\tilde{X}\,^2\Sigma^+$ transition (in cm^{-1}).

N	$P_1(N)$	$\Delta\nu$[a]	$P_2(N)$	$\Delta\nu$	$R_1(N)$	$\Delta\nu$	$R_2(N)$	$\Delta\nu$
0					13 200.379	−0.012		
1					13 200.750	−0.008	13 200.974	−0.010
2					13 201.112	−0.007	13 201.429	−0.003
3	13 198.587	−0.003			13 201.470	−0.003	13 201.870	−0.003
4	13 198.082	−0.003	13 198.399	−0.004	13 201.819	−0.001	13 202.310	0.004
5			13 197.976	−0.001	13 202.163	0.003	13 202.740	0.007
6	13 197.058	0.005			13 202.497	0.004		
7	13 196.532	0.006	13 197.110	0.005	13 202.823	0.004	13 203.569	0.008
8	13 195.996	0.003	13 196.660	0.003	13 203.142	0.005	13 203.970	0.006
9	13 195.457	0.004	13 196.205	0.004	13 203.456	0.006	13 204.360	0.003
10	13 194.909	0.002	13 195.743	0.006	13 203.759	0.004	13 204.744	0.004
11	13 194.357	0.005	13 195.265	0.000	13 204.057	0.004	13 205.117	0.002
12	13 193.791	0.000	13 194.783	0.000	13 204.349	0.005	13 205.480	0.001
13	13 193.231	0.007	13 194.292	0.000	13 204.634	0.007	13 205.832	−0.001
14	13 192.653	0.004	13 193.787	−0.004	13 204.910	0.005	13 206.173	−0.002
15	13 192.068	0.001	13 193.272	−0.006	13 205.177	0.002	13 206.506	0.000
16	13 191.476	−0.003	13 192.747	−0.009	13 205.438	0.000	13 206.821	−0.003
17	13 190.884	0.000	13 192.212	−0.009	13 205.696	0.002	13 207.129	0.000
18	13 190.279	−0.003	13 191.664	−0.009	13 205.940	−0.002	13 207.418	−0.002
19			13 191.104	−0.008	13 206.178	−0.007	13 207.693	−0.002
20	13 189.056	0.000	13 190.530	−0.008	13 206.415	−0.004	13 207.959	0.004
21	13 188.436	0.002	13 189.946	−0.004	13 206.641	−0.006	13 208.201	0.002
22	13 187.804	0.000	13 189.340	−0.005	13 206.863	−0.005	13 208.431	0.006
23	13 187.167	0.000	13 188.727	0.003	13 207.079	−0.002	13 208.640	0.008
24			13 188.091	0.005	13 207.284	−0.004	13 208.824	0.003
25	13 185.866	−0.007	13 187.439	0.009	13 207.483	−0.005	13 208.990	0.001
26	13 185.210	−0.005	13 186.764	0.011	13 207.674	−0.006	13 209.138	0.003
27	13 184.547	−0.004			13 207.860	−0.005	13 209.356	−0.004
28	13 183.874	−0.006			13 208.039	−0.004	13 209.345	−0.014
29	13 183.193	−0.009			13 208.207	−0.008		
30					13 208.374	−0.005		
31	13 181.827	0.002			13 208.534	−0.002		
32	13 181.129	0.003			13 208.685	−0.001		
33	13 180.426	0.006			13 208.829	0.001		
34	13 179.713	0.004			13 208.965	0.002		
35	13 178.992	0.003			13 209.094	0.002		
36	13 178.267	0.004			13 209.217	0.004		
37	13 177.532	0.003			13 209.332	0.005		
38					13 209.439	0.005		
39					13 209.538	0.004		
40	13 175.293	0.005			13 209.629	0.003		
41	13 174.534	0.007			13 209.715	0.004		
42					13 209.791	0.002		
43	13 172.990	0.006			13 209.857	−0.003		
44	13 172.207	0.004			13 209.913	−0.010		
45	13 171.417	0.002						
46	13 170.613	−0.006						
47					13 210.072	0.003		
48								
49	13 168.196	0.005						
50	13 167.364	−0.003						
51	13 166.526	−0.011						

[a] $\Delta\nu$ is observed-calculated.

$$\mathrm{Ba} + \mathrm{H_2O} \xrightarrow{\mathrm{Ar}} \mathrm{H\text{–}Ba\text{–}OH}$$

$$\mathrm{H\text{–}Ba\text{–}OH} + \mathrm{Ba} \rightarrow \mathrm{BaH} + \mathrm{BaOH}$$

$$\mathrm{BaH} + \mathrm{H_2O} \rightarrow \mathrm{BaOH} + \mathrm{H_2}$$

$$\mathrm{Ba} + \mathrm{H_2O} \rightarrow \mathrm{BaOH} + 1/2\mathrm{H_2}$$

and

$$\mathrm{Ba} + \mathrm{H_2O} \xrightarrow{\mathrm{Ar}} \mathrm{H\text{–}Ba\text{–}OH}$$

$$\mathrm{H\text{–}Ba\text{–}OH} + \mathrm{H_2O} \rightarrow \mathrm{Ba(OH)_2} + \mathrm{H_2}$$

$$\mathrm{Ba(OH)_2} + \mathrm{Ba} \rightarrow 2\mathrm{BaOH}$$

$$\mathrm{Ba} + \mathrm{H_2O} \rightarrow \mathrm{BaOH} + 1/2\mathrm{H_2}$$

These proposed mechanisms explain why a higher total pres-

TABLE IV. The measured lines of the BaOH 001–000 $\tilde{B}\,^2\Sigma^+$–$\tilde{X}\,^2\Sigma^+$ transition (in cm^{-1}).

N	$P_1(N)$	$\Delta\nu$[a]	$P_2(N)$	$\Delta\nu$	$R_1(N)$	$\Delta\nu$	$R_2(N)$	$\Delta\nu$
0					13 661.351	−0.003		
1					13 661.661	−0.003		
2	13 660.052	−0.001			13 661.959	−0.003		
3	13 659.497	0.002			13 662.248	−0.001		
4	13 658.931	0.003	13 659.709	0.012	13 662.526	0.000	13 663.692	0.001
5	13 658.349	0.000	13 659.322	0.003	13 662.793	0.002	13 664.157	−0.001
6	13 657.760	0.001	13 658.930	0.000	13 663.047	0.000	13 664.609	−0.004
7	13 657.160	0.002	13 658.525	−0.004	13 663.294	0.003	13 665.054	−0.003
8	13 656.547	−0.001	13 658.115	−0.004	13 663.527	0.002	13 665.487	−0.004
9			13 657.695	−0.002	13 663.749	0.001	13 665.911	−0.002
10	13 655.294	0.000	13 657.262	−0.003	13 663.961	0.001	13 666.323	−0.002
11	13 654.651	0.000	13 656.822	0.000	13 664.161	0.000	13 666.722	−0.004
12	13 653.997	0.000	13 656.365	−0.002	13 664.351	0.000	13 667.112	−0.004
13	13 653.328	−0.003			13 664.532	0.000	13 667.492	−0.002
14	13 652.657	0.000	13 655.429	0.002	13 664.702	0.001	13 667.862	0.001
15	13 651.970	−0.002	13 654.943	0.003	13 664.859	0.000	13 668.219	0.001
16	13 651.274	−0.001	13 654.444	0.002	13 665.008	0.001	13 668.565	0.002
17	13 650.563	−0.005	13 653.938	0.005	13 665.146	0.002	13 668.899	0.002
18	13 649.848	−0.003	13 653.417	0.004	13 665.273	0.002	13 669.224	0.004
19	13 649.122	−0.001	13 652.882	0.001	13 665.390	0.003	13 669.533	0.002
20	13 648.380	−0.005	13 652.340	0.001	13 665.495	0.002	13 669.832	0.002
21	13 647.634	−0.003	13 651.789	0.004	13 665.590	0.002	13 670.120	0.001
22	13 646.875	−0.002	13 651.225	0.005	13 665.674	0.000	13 670.393	−0.003
23	13 646.108	0.000	13 650.645	0.000	13 665.750	0.002	13 670.658	−0.003
24	13 645.325	−0.003	13 650.057	0.000	13 665.813	0.002	13 670.915	0.001
25	13 644.536	−0.002	13 649.457	0.000	13 665.865	0.000	13 671.157	0.001
26	13 643.739	0.000	13 648.849	0.002	13 665.905	−0.003	13 671.388	0.003
27	13 642.927	−0.001	13 648.225	0.000	13 665.940	−0.001	13 671.605	0.002
28	13 642.109	0.000	13 647.589	−0.001	13 665.967	0.002	13 671.810	0.000
29	13 641.279	0.001	13 646.943	−0.002	13 665.978	0.001	13 672.001	−0.002
30	13 640.439	0.002	13 646.285	−0.003	13 665.981	0.002	13 672.184	−0.001
31			13 645.618	−0.001	13 665.974	0.002	13 672.353	−0.001
32	13 638.727	0.000	13 644.935	−0.003	13 665.956	0.002	13 672.506	−0.005
33	13 637.857	0.001	13 644.243	−0.002	13 665.926	0.000	13 672.650	−0.006
34	13 636.976	−0.001	13 643.538	−0.002	13 665.888	0.000	13 672.787	−0.001
35	13 636.087	0.000	13 642.821	−0.001			13 672.904	−0.004
36	13 635.183	−0.004	13 642.093	0.000			13 673.015	0.001
37			13 641.350	0.000			13 673.108	−0.001
38			13 640.597	0.001			13 673.189	−0.001
39			13 639.830	0.001			13 673.258	0.000
40			13 639.053	0.004			13 673.315	0.003
41			13 638.260	0.003			13 673.357	0.003
42			13 637.455	0.004			13 673.386	0.004
43			13 636.638	0.005				
44			13 635.805	0.004				
45			13 634.956	0.000				
46			13 634.097	−0.002				
47			13 633.217	−0.010				

[a] $\Delta\nu$ is observed–calculated.

sure in the oven enhances molecule production since a third body (Ar) is required to produce H–Ba–OH. (At higher pressures more H–Ba–OH intermediate is formed.)

The H–Ba–OH molecule has been detected by infrared absorption in matrix isolation experiments.[35] Since H–Ba–OH probably has a UV absorption spectrum, it was not observed in our visible laser experiments. BaH was detected in our organometallic experiments[55] when formic and acetic acids were used as oxidants, but was not observed in the present experiments possibly because of fast reaction with excess H_2O oxidant. The absence of BaH tends to favor the second mechanism but this is not conclusive evidence.

B. Perturbations

The $\tilde{B}\,^2\Sigma^+$ states of BaOH and BaOD are badly perturbed, most likely by vibrational levels of the $\tilde{A}\,^2\Pi$ state. The strong $\tilde{B}\,^2\Sigma^+ \sim \tilde{A}\,^2\Pi$ interaction is evident from a number of unusual effects in the spectra. The simplest to understand is the observation of a local perturbation in the f levels ($N' \simeq 40$) of the $\tilde{B}\,^2\Sigma^+$ 000 state of BaOD caused by a level crossing.

Extra features are observed in the broadband laser excitation spectra (Figs. 1 and 2). These are most likely due to $\tilde{A}\,^2\Pi$ vibrational levels with poor $\tilde{A}$–$\tilde{X}$ Franck–Condon fac-

TABLE V. The measured lines of the BaOD 000–000 $\tilde{B}\,^2\Sigma^+$–$\tilde{X}\,^2\Sigma^+$ transition (in cm^{-1}).

N	$P_1(N)$	$\Delta\nu$[a]	$P_2(N)$	$\Delta\nu$	$R_1(N)$	$\Delta\nu$	$R_2(N)$	$\Delta\nu$
3								
4							13 176.404	0.005
5			13 172.419	0.013			13 176.864	−0.001
6			13 172.100	0.005	13 174.735	−0.017	13 177.318	−0.005
7			13 171.777	−0.001			13 177.767	−0.006
8	13 168.865	−0.013	13 171.450	−0.003	13 175.136	−0.004	13 178.208	−0.008
9	13 168.289	−0.005	13 171.122	0.001	13 175.320	0.000	13 178.644	−0.009
10			13 170.774	−0.008	13 175.499	0.010	13 179.078	−0.004
11	13 167.107	0.010	13 170.433	−0.003	13 175.659	0.010	13 179.504	0.001
12	13 166.495	0.011	13 170.078	−0.003	13 175.809	0.009	13 179.919	0.001
13	13 165.869	0.007	13 169.719	−0.002	13 175.948	0.007	13 180.324	0.000
14			13 169.353	0.000	13 176.077	0.004	13 180.727	0.004
15	13 164.591	0.002	13 168.976	0.000	13 176.197	0.003	13 181.118	0.004
16	13 163.937	0.000	13 168.595	0.003	13 176.307	0.001	13 181.503	0.005
17	13 163.278	0.002	13 168.205	0.004	13 176.407	−0.001	13 181.878	0.005
18			13 167.806	0.003	13 176.497	−0.005	13 182.247	0.006
19			13 167.399	0.003	13 176.582	−0.004	13 182.606	0.006
20			13 166.983	0.001	13 176.651	−0.008	13 182.956	0.004
21			13 166.561	0.002	13 176.716	−0.008	13 183.299	0.004
22			13 166.130	0.000	13 176.770	−0.009	13 183.630	0.000
23			13 165.692	0.001	13 176.818	−0.008	13 183.950	−0.007
24			13 165.237	−0.007	13 176.856	−0.005	13 184.277	0.002
25			13 164.779	−0.010			13 184.584	0.001
26			13 164.319	−0.006			13 184.885	0.001
27			13 163.853	0.000			13 185.173	−0.002
28			13 163.371	−0.001			13 185.454	−0.003
29			13 162.877	−0.005			13 185.728	−0.001
30							13 185.992	−0.001
31			13 161.873	−0.003			13 186.247	0.000
32			13 161.358	−0.001	13 176.824	−0.002	13 186.491	0.000
33					13 176.779	−0.002	13 186.725	0.000
34					13 176.726	−0.002	13 186.953	0.004
35			13 159.756	0.005	13 176.666	0.001	13 187.164	0.000
36			13 159.201	0.006	13 176.593	−0.001	13 187.361	−0.006
37					13 176.518	0.004		
38			13 158.054	0.000	13 176.431	0.005		
39					13 176.336	0.006		
40					13 176.229	0.005		
41					13 176.117	0.006		
42					13 175.994	0.005		
43					13 175.860	0.001		
44					13 175.718	−0.002		
45					13 175.567	−0.007		
46					13 175.412	−0.008		

[a] $\Delta\nu$ is observed–calculated.

tors which mix with nearby $\tilde{B}\,^2\Sigma^+$ vibrational levels and appear by intensity borrowing.

The 000–010 $\tilde{B}\,^2\Sigma$–$\tilde{X}\,^2\Sigma^+$ band was observed with about the same intensity as the 000–020 band. This is also evidence for strong $\tilde{B}\,^2\Sigma^+ \sim \tilde{A}\,^2\Pi$ vibronic interactions. The bending vibration has π symmetry, hence the vibrational part of the transition dipole integral[56]:

$$R_{e'e''v'v''} = R_{e'e''} \int \psi_v'^{*}\, \psi_v''\, d\tau \qquad (1)$$

is not totally symmetric for the 000–010 band. Within the Born–Oppenheimer approximation, therefore, the 000–010 band is forbidden. Neglected terms in the complete Hamiltonian mix the electronic and vibrational wave functions so Eq. (1) no longer applies. In particular, the $\tilde{B}\,^2\Sigma^+$ 000 (Σ)

TABLE VI. Observed molecular constants for BaOH $\tilde{B}\,^2\Sigma^+$–$\tilde{X}\,^2\Sigma^+$ transitions (in cm^{-1}).

	$\tilde{X}\,^2\Sigma^+$ 000	$\tilde{B}\,^2\Sigma^+$ 000		$\tilde{B}\,^2\Sigma^+$ 001	
		$P_1,R_1(e)$	$P_2,R_2(f)$	$P_1,R_1(e)$	$P_2,R_2(f)$
T_v	0	13 200.015(2)[a]	13 200.033(4)	13 661.033(2)	13 661.101(3)
B_v	0.216 571(11)	0.213 104(15)	0.213 152(43)	0.211 175(23)	0.211 184(18)
D_v	$1.521(41)\times10^{-7}$	$1.588(49)\times10^{-7}$	$1.885(24)\times10^{-6}$	$8.38(93)\times10^{-8}$	$2.666(56)\times10^{-7}$
γ_v	0.002 70(50)	−0.100 59(76)	−0.068 4(17)	−0.202 4(10)	−0.193 05(95)

[a] Numbers in parentheses correspond to one standard deviation.

TABLE VII. Observed molecular constants for the BaOD $\tilde{B}\,^2\Sigma^+$–$\tilde{X}\,^2\Sigma^+$ transition (in cm^{-1}).

	$\tilde{X}\,^2\Sigma^+$ 000	$\tilde{B}\,^2\Sigma^+$ 000	
		$P_1,R_1(e)$	$P_2,R_2(f)$
T_v	0	13 173.086(7)	13 173.851(6)
B_v	0.195 743(32)[a]	0.190 861(44)	0.192 211(47)
D_v	$1.09(18)\times10^{-7}$	$3.5(18)\times10^{-8}$	$3.12(21)\times10^{-7}$
γ_v	0.002 44[b]	−0.226 6(19)	−0.230 3(18)

[a] Numbers in parentheses correspond to one standard deviation.
[b] Estimated and fixed. See the text for details.

vibronic state interacts with $\tilde{A}\,^2\Pi(\Sigma)$ vibronic states [e.g., 010 (Σ)], the $\tilde{B}\,^2\Sigma^+$–$\tilde{X}\,^2\Sigma^+$ 000–010 transition is observed because of intensity borrowing.[56] "Spin-orbit vibronic" coupling[57] is probably responsible for the strength of the 000–010 transition in BaOH.[45]

Finally, the most unusual and interesting observation is that a separate set of spectroscopic constants are required for the e and the f levels of the $\tilde{B}\,^2\Sigma^+$ state. This is surprising since the Hamiltonian explicitly contains the terms which take into account the interaction of a remote $^2\Pi$ state with a $^2\Sigma$ state. The matrix elements derived by second-order perturbation theory are[58]

$$H^{(2)}_{1/2\,1/2}(e) = o_v^\Sigma - \tfrac{1}{2}p_v^\Sigma(J-\tfrac{1}{2}) + q_v^\Sigma(J-\tfrac{1}{2})(J+\tfrac{1}{2}),$$

$$H^{(2)}_{1/2\,1/2}(f) = o_v^\Sigma + \tfrac{1}{2}p_v^\Sigma(J+\tfrac{3}{2}) + q_v^\Sigma(J+\tfrac{1}{2})(J+\tfrac{3}{2}). \quad (2)$$

The only parity dependent term is the second-order contribution to the spin-rotation interaction, $\gamma_v^{(2)} \equiv -p_v^\Sigma$. The o_v^Σ and q_v^Σ parameters shift the band origin and the rotational constant, respectively, and hence affect e and f levels equally.

The electronic states of BaOH can be derived by analogy with the isoelectronic BaF molecule.[46,59] BaOH is an ionic molecule well represented by the Ba^+OH^- structure. The remaining 6s valence electron on Ba^+ is perturbed by the OH^- ligand. The $\tilde{X}\,^2\Sigma^+$ state is largely 6$s\sigma$ while the $\tilde{A}\,^2\Pi$ and $\tilde{B}\,^2\Sigma^+$ states are 6$p\pi$, 5$d\pi$ and 6$p\sigma$, 5$d\sigma$ mixtures, respectively.

The $\tilde{A}$ and $\tilde{B}$ states arise from the promotion of a Ba^+ electron from a 6s to a 6p orbital (each with considerable 5d character) and can be considered a unique perturber pair[58] connected by the $B(r)(J_+L_- + J_-L_+)$, and $[A(r)/2 + B(r)]\,(L_+S_- + L_-S_+)$ operators ($A = 635\ cm^{-1}$ for the $\tilde{A}\,^2\Pi$ state). This strong, distant interaction between the 000 levels of the $\tilde{B}\,^2\Sigma^+$ and $\tilde{A}\,^2\Pi$ states produces a large negative γ value in the $\tilde{B}\,^2\Sigma^+$ state.

In addition to the strong, distant interaction which separates the e and f levels, there are local $\tilde{B}\,^2\Sigma^+ \sim \tilde{A}\,^2\Pi$ interactions when two vibronic states are near each other but do not actually cross. This local interaction causes a parity dependence in the constants because the e–e energy level separation is different from the f–f energy level separation.

The definition[58] of o_v^Σ [Eq. (2)] illustrates qualitatively how the separate e and f constants arise. Although perturbation theory is not very suitable for two nearby vibronic states, it provides some physical insight.

$$o_v^{\Sigma*} \equiv \sum_{\substack{n'v' \\ v'\neq v}} \frac{\langle n'\,^2\Pi v' J|\tfrac{1}{2}A(r)L_+|n\,^2\Sigma^+ v J\rangle^2}{E_{nvJ} - E_{n'v'J}}$$

$$\simeq \frac{\langle \tilde{A}\,^2\Pi_{1/2} v' J|\tfrac{1}{2}A(r)L_+|\tilde{B}\,^2\Sigma^+ v J\rangle^2}{E_{vJ} - E_{v'J}} \quad (3)$$

$$\simeq \frac{\tfrac{1}{2}\langle AL_+\rangle^2\langle v'|v\rangle^2}{E_{vJ} - E_{v'J}}.$$

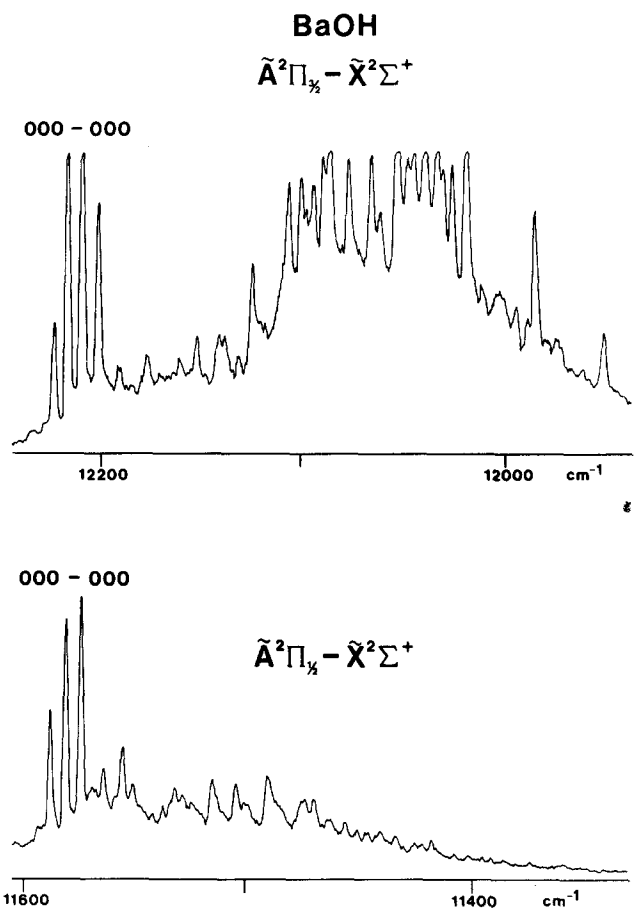

FIG. 6. BaOH $\tilde{A}\,^2\Pi$–$\tilde{X}\,^2\Sigma^+$ fluorescence. When the single frequency dye laser was on the $R_1(15)$ rotational line of the BaOH $\tilde{B}\,^2\Sigma^+$–$\tilde{X}\,^2\Sigma^+$ 000–000 band (13 205.177 cm^{-1}), fluorescence was observed for the $\tilde{A}\,^2\Pi$–$\tilde{X}\,^2\Sigma^+$ transition. Overlapped rotational lines in the 000–000 band were observed due to resonant $\tilde{B}\,^2\Sigma^+$–$\tilde{A}\,^2\Pi$–$\tilde{X}\,^2\Sigma^+$ cascade. The signal decreases near 11 500 cm^{-1} as the red limit of the photomultiplier is reached.

TABLE VIII. Ground state vibrational frequencies for BaOH, BaOD, and similar molecules (in cm^{-1}).

	BaOX[a]	SrOX	CaOX[d]	MgOX[e]
X = H				
ν_2(M–O–H)	341.6(6)	361(1)[b]	339(1)	185
ν_3(M–O)	492.4(8)	528(1)	606(1)	
X = D				
ν_2(M–O–D)	257.6(4)	282(10)[c]	240(1)	128
ν_3(M–O)	482.4(2)	510(10)	603(1)	

[a] This work. Numbers in parentheses correspond to one standard deviation in the last digit.
[b] Reference 45.
[c] Reference 42.
[d] Reference 41.
[e] Reference 61.

The strong distant $\tilde{B}\sim\tilde{A}$ interaction has been removed from Eq. (3). (o_v^Σ contains only distant $v'=v''$ interactions, $\langle v|v\rangle\simeq 1$, while $o_v^{\Sigma *}$ contains a local interaction.) The overlap integral, $\langle v'|v\rangle$, between the 000 level of the $\tilde{B}\,^2\Sigma^+$ state and excited vibrational levels of the $\tilde{A}\,^2\Pi$ state is likely to be small. As a result only one nearby vibronic level of the $\tilde{A}$ state, for which $E_{vJ}-E_{v'J}$ is also small, is likely to be important. The parity dependence appears in the denominator of Eq. (3):

$$o_v^{\Sigma *}\simeq \frac{\frac{1}{2}\langle AL_+\rangle^2\langle v'|v\rangle^2}{\Delta E\pm(\gamma/2)(N+\frac{1}{2})\pm(p/2)(J+\frac{1}{2})}$$

$$\simeq \frac{\frac{1}{2}\langle AL_+\rangle^2\langle v'|v\rangle^2}{\Delta E}\left[1\mp\frac{\gamma}{\Delta E}(N+\tfrac{1}{2})\right], \qquad (4)$$

where the upper/lower sign refers to the e/f levels, and $\gamma\simeq p$ because the $\tilde{A}$ and $\tilde{B}$ states form a unique perturber pair with similar rotational constants. The term

$$\mp o_v^\Sigma\langle v'|v\rangle^2\frac{\gamma}{\Delta E}(N+\tfrac{1}{2})$$

introduces parity dependence linear in N. For values of $o_v^\Sigma=124\ cm^{-1}$ (pure precession[58,60]), $\langle v'|v\rangle^2=0.01$, $\gamma=p=-0.2$ a ΔE of about $10\ cm^{-1}$ is required for the 000 $\tilde{B}\,^2\Sigma^+$ state. This leads to a different spin-rotation constant for the e and f levels. In a similar fashion, the second term in Eq. (2) produces a small parity dependence in the rotational constant.

$$\mp p_v^\Sigma\langle v'|v\rangle^2\frac{\gamma}{\Delta E}N(N+1).$$

Using the same parameters as above with $\Delta E=10\ cm^{-1}$ $B_{000e}-B_{000f}$ is predicted to be $8\times10^{-5}\ cm^{-1}$ compared with the observed $5\times10^{-5}\ cm^{-1}$ for BaOH. The BaOD 000 $\tilde{B}\,^2\Sigma^+$ data are rather different since $\gamma_e\simeq\gamma_f$ while the band origins and B_e and B_f values differ substantially. Unlike the less perturbed BaOH, the "$\tilde{B}\,^2\Sigma^+$ 000e" and "$\tilde{B}\,^2\Sigma^+$ 000f" may not both originate from the same vibronic parent state ($\tilde{B}\,^2\Sigma^+$ 000). Leftover N independent terms introduce a parity dependence into the origin. For $l=1$, the pure precession values[60] of p and γ are

$$p_0\simeq\gamma_0=\frac{4A_0B_0}{E_0(\tilde{A}\,^2\Pi_{1/2})-E_0(\tilde{B}\,^2\Sigma^+)}=-0.3325\ cm^{-1}. \qquad (5)$$

C. Comparisons

The known ground state vibrational frequencies of the alkaline earth monohydroxides are listed in Table VIII. The bending frequency ν_2 drops for MgOH[61] because of quasilinear tendencies: the bonding is becoming more covalent so the bottom of the bending potential curve flattens out. The frequency changes in ν_2 upon deuteration are consistent with the Teller–Redlich product rule.[62]

The metal–oxygen stretches (ν_3) decrease only slightly upon deuteration. As the mass of the metal increases the metal–oxygen stretching frequency decreases. Treating the OH^- or OD^- as a single mass one can compute a metal–ligand "reduced" mass. For the three points available, a plot of observed vibrational frequency against the square root of the reciprocal of this pseudodiatomic reduced mass produces a straight line. The predicted Mg–O stretching frequency is $702\ cm^{-1}$. This empirical correlation suggests that the M–O force constant is similar for the ionically bonded alkaline earth monohydroxides.

The known bond lengths of the alkaline earth monohydroxides are listed in Table IX. The O–H r_0 bond lengths are approximately the same while the M–O bond length increases regularly by about 0.1 Å for each metal in the CaOH, SrOH, and BaOH series.

CONCLUSIONS

The first high-resolution observations of BaOH prove that this radical is linear, like the other alkaline earth monohydroxides. The $\tilde{B}\,^2\Sigma^+$–$\tilde{X}\,^2\Sigma^+$ transitions of BaOH and BaOD were rotationally analyzed and an r_0 structure was established. Laser induced fluorescence spectra provided vibrational frequencies. The $\tilde{B}\,^2\Sigma^+$ state was found to be hea-

TABLE IX. Ground state bond lengths for BaOH and similar molecules (in Å).

	BaOH[a]	SrOH[b]	CaOH[c]
r_0(M–O)	2.201	2.111	1.986
r_0(O–H)	0.923	0.922	0.901

[a] This work.
[b] Reference 42.
[c] Reference 41.

vily perturbed by the $\tilde{A}\,^2\Pi$ state and separate spectroscopic constants were required for the e and f parity levels of the $\tilde{B}$ state.

ACKNOWLEDGMENTS

This research was supported by grants from the National Science Foundation (CHE-8306504) and the Research Corporation. Acknowledgment is made to the donors of the Petroleum Research Fund, administered by the ACS, for partial support of this research.

[1]C. Th. J. Alkemade, Tj. Hollander, W. Snelleman, and P. J. Th. Zeegers, *Metal Vapours in Flames* (Pergamon, Oxford, 1982).
[2]T. Tsuji, Astron. Astrophys. **23**, 411 (1973).
[3]P. Pesch, Astrophys. J. Lett. **174**, L155 (1974).
[4]E. Murad, W. Swider, and S. W. Benson, Nature **289**, 273 (1981).
[5]S. Drapatz, L. Haser, and K. W. Michel, Z. Naturforsch. A **29**, 411 (1974).
[6]S. C. Liu and G. C. Reid, Geophys. Res. Lett. **6**, 283 (1979).
[7]E. Murad and W. Swider, Geophys Res. Lett. **6**, 929 (1979).
[8]D. Smith, N. G. Adams, E. Alge, and E. Herbst, Astrophys. J. **272**, 365 (1983).
[9]W. W. Duley and T. J. Millar, Astrophys. J. **220**, 124 (1978).
[10]J. F. W. Herschel, Trans. R. Soc. (Edinburgh) **9**, 445 (1823).
[11]C. G. James and T. M. Sugden, Nature **175**, 333 (1955)
[12]M. Charton and A. G. Gaydon, Proc. Phys. Soc. London Sect. A **69**, 520 (1956).
[13]A. G. Gaydon, Proc. Soc. London, Ser. A **231**, 437 (1955).
[14]J. Van Der Hurk, Tj. Hollander, and C. Th. J. Alkemade, J. Quant. Spectrosc. Radiat. Transfer **13**, 273 (1973); **14**, 1167 (1974).
[15]H. G. C. Human and P. J. Th. Zeegers, Spectrochim. Acta Part B **30**, 203 (1975).
[16]S. J. Weeks, H. Haraguchi, and J. D. Winefordner, J. Quant. Spectrosc. Radiat. Transfer **19**, 633 (1978).
[17]M. B. Blackburn, J. M. Mermet, and J. D. Winefordner, Spectrochim. Acta Part A **34**, 847 (1978).
[18]H. Haraguchi, S. J. Weeks, and J. D. Winefordner, Spectrochim. Acta Part A **35**, 391 (1979).
[19]J. M. Goodings and S. M. Graham, Int. J. Mass Spectrom. Ion Processes **56**, 193 (1984).
[20]D. H. Cotton and D. R. Jenkins, Trans. Faraday Soc. **67**, 730 (1971).
[21]B. S. Hayes, H. Jander, H. Mätzing, and H. G. Wagner, Comb. Flame **40**, 101 (1981).
[22]E. M. Bulewicz and T. M. Sugden, Trans. Faraday Soc. **55**, 720 (1959).
[23]L. V. Gurvich, V. G. Ryabova, and A. N. Khitrov, Faraday Symp. Chem. Soc. **8**, 83 (1973).
[24]R. Kelley and P. J. Padley, Trans. Faraday Soc. **67**, 1384 (1971).
[25]A. N. Hayhurst and D. B. Kittelson, Comb. Flame **19**, 306 (1972).
[26]E. Murad, Chem. Phys. Lett. **72**, 295 (1980); J. Chem. Phys. **75**, 4080 (1981).
[27]A. N. Hayhurst and D. B. Kittelson, Proc. R. Soc. London Ser. A **338**, 175 (1974).
[28]E. Murad, J. Chem. Phys. **77**, 2057 (1982); **78**, 6611 (1983).
[29]B. R. Rowe, D. W. Fahey, E. E. Ferguson, and F. C. Fehsenfeld, J. Chem. Phys. **75**, 3325 (1981).
[30]J. M. Brom, Jr. and W. Weltner, Jr., J. Chem. Phys. **58**, 5322 (1973); **64**, 3894 (1976).
[31]A. Hinchliffe, J. Mol. Struct. **64**, 289 (1980).
[32]Yu. G. Abashkin and A. I. Dement'ev, J. Struct. Chem. **23**, 152 (1982).
[33]W. E. Palke and B. Kirtman, Chem. Phys. Lett. **117**, 424 (1985).
[34]C. W. Bauschlicher, Jr., and H. Partridge, Chem. Phys. Lett. **106**, 65 (1984).
[35]J. W. Kauffman, R. H. Hauge, and J. L. Margrave, High Temp. Sci. **18**, 97 (1984).
[36]D. Pesic and A. G. Gaydon, Proc. Phys. Soc. London Sect. A **73**, 244 (1959).
[37]L. Brewer and S. Trajmar, J. Chem. Phys. **36**, 1585 (1962).
[38]D. J. Benard, W. D. Slafer, and J. Hecht, J. Chem. Phys. **66**, 1012 (1977).
[39]R. F. Wormsbecher, M. Trkula, C. Martner, R. E. Penn, and D. O. Harris, J. Mol. Spectrosc. **97**, 29 (1983).
[40]J. B. West, R. S. Bradford, J. D. Eversole, and C. R. Jones, Rev. Sci. Instrum. **46**, 164 (1975).
[41]R. C. Hilborn, Zhu Qingshi, and D. O. Harris, J. Mol. Spectrosc. **97**, 73 (1983).
[42]J. Nakagawa, R. F. Wormsbecher, and D. O. Harris, J. Mol. Spectrosc. **97**, 37 (1983).
[43]P. F. Bernath and S. Kinsey-Nielsen, Chem. Phys. Lett. **105**, 663 (1984).
[44]P. F. Bernath and C. R. Brazier, Astrophys. J. **288**, 373 (1985).
[45]C. R. Brazier and P. F. Bernath, J. Mol. Spectrosc. (in press).
[46]R. F. Barrow, M. W. Bastin, and B. Longborough, Proc. Phys. Soc. (London) **92**, 518 (1967).
[47]P. C. F. Ip, P. F. Bernath, and R. W. Field, J. Mol. Spectrosc. **89**, 53 (1981).
[48]C. Linton, J. Mol. Spectrosc. **69**, 351 (1978).
[49]M. Dulick, P. F. Bernath, and R. W. Field, Can. J. Phys. **58**, 703 (1980).
[50]B. A. Palmer and R. Engleman, Jr., LANL Rep. LA-9615, Los Alamos National Laboratory, Los Alamos, NM, 1983.
[51]C. J. Sansonetti and K. H. Weber, J. Opt. Soc. Am. B **1**, 361 (1984).
[52]R. S. Mulliken, J. Chem. Phys. **23**, 1997 (1955).
[53]G. Herzberg, *Spectra of Diatomic Molecules* (Van Nostrand, Princeton, 1950).
[54]J. M. Brown *et al.*, J. Mol. Spectrosc. **55**, 500 (1975).
[55]C. R. Brazier, P. F. Bernath, S. Kinsey-Nielsen, and L. C. Ellingboe, J. Chem. Phys. **82**, 1043 (1985).
[56]G. Herzberg, *Electronic Spectra and Electronic Structure of Polyatomic Molecules* (Van Nostrand–Reinhold, New York, 1966).
[57]G. Fischer, *Vibronic Coupling* (Academic, Orlando, FL, 1984), p. 134.
[58]R. N. Zare, A. L. Schmeltekopf, W. J. Harrop, and D. L. Albritton, J. Mol. Spectrosc. **43**, 37 (1973).
[59]S. F. Rice, H. Martin, and R. W. Field, J. Chem. Phys. **82**, 5073 (1985).
[60]R. S. Mulliken and A. Christy, Phys. Rev. **38**, 87 (1931).
[61]Yong Ni and D. O. Harris (private communication).
[62]G. Herzberg, *Infrared and Raman Spectra* (Van Nostrand, New York, 1945), p. 231.